The Role of Nitrogen on the Deformation Response of Hadfield Steel Single Crystals

D. CANADINC, I. KARAMAN, H. SEHITOGLU, Y.I. CHUMLYAKOV, and H.J. MAIER

We studied the role of nitrogen content on the stress-strain response of Hadfield steel (HS) single crystals under compressive loading. Two different nitrogen concentrations were examined for each orientation (0.05 wt pct and 1.06 wt pct) with drastic increase in critical resolved shear stresses (CRSSs) and strain-hardening coefficients compared to HS without nitrogen. The stress-strain response was strongly dependent on both the crystallographic orientation and the nitrogen concentration. Transmission electron microscopy (TEM) results revealed that, for the HS with 1.06 wt pct nitrogen, the hardening is influenced by the coexisting deformation twins and precipitates, which both act as strong obstacles against dislocation motion. A visco-plastic self-consistent (VPSC) model was modified to account for precipitation and twinning length scales in HS with 1.06 wt pct nitrogen for selected crystallographic orientations. Incoherent precipitates in the hardening formulation were treated as factors affecting the mean free path of dislocations. The model also accounts for plastic relaxation of precipitates with increasing strain and accurately predicts the stress-strain response.

I. INTRODUCTION

RECENT developments in nitrogen steel processing technologies have led to an increased use of nitrogen alloying as a strengthening mechanism for steels.[1,2] By alloying with nitrogen, which is a strong austenite stabilizer, solid solution hardening is obtained without a significant loss of fracture toughness. Possessing a higher solubility than carbon in austenitic iron forming and stronger substitutional-interstitial (s-i) atom couples, nitrogen is preferably used for the strengthening of austenitic stainless steels.[3,4,5]

Most of the previous work on the strengthening of steels by nitrogen alloying was conducted on austenitic stainless steels. It has been reported that flow stress in austenitic stainless steels increases with increasing nitrogen concentration, which also influences the thermally activated component of the flow stress.[4,5] Similar observations were made in single crystals.[2,6–9] In our previous studies, we investigated Hadfield steel (HS) (an austenitic manganese steel) single crystals under compression and tension. The unusual strain-hardening behavior of HS was attributed to interstitial solid solution hardening, early activation of deformation twinning, slip-twin interaction, and dynamic strain aging of Mn-C couples.[10,11]

The present study is undertaken to investigate the effect of nitrogen on the critical resolved shear stresses (CRSS) of slip and twinning, different stages of deformation, strain-hardening coefficients, and the deformation mechanisms of HS. These observations are necessary because nitrogen is more soluble than carbon, and Mn-N s-i atom couples are stronger than Mn-C couples.[12] Therefore, a difference in the strain-hardening behavior and deformation mechanisms of Hadfield steel is expected due to the nitrogen addition. The addition of nitrogen in single crystals will also change the extent of slip and twinning.

The consideration of slip and twinning together as governing deformation mechanisms in the crystal plasticity models has gained considerable attention in the last decade.[13,14,15] The main shortcomings of current crystal plasticity models are the lack of (1) incorporation of twinning and precipitates into models as a deformation mechanism or a microstructural feature that strongly affects the deformation and monitoring the texture evolution due to abrupt orientation change by twinning and anisotropy change due to precipitates; (2) understanding of slip-twin interaction on the stress-strain response and incorporating this into a mathematical framework; and (3) a physical basis for the relation between deformation length scales (grain size, twin thickness, precipitate size, morphology and volume fraction, localized deformation zones, *etc.*) and dislocation density evolution, and thus strain hardening.

We have recently introduced a unique strain-hardening approach within a visco-plastic self-consistent crystal plasticity framework incorporating length scales associated with spacing between twin lamellae and grain boundaries.[2,16,17] Twin boundaries are treated as hard but penetrable obstacles. The model successfully predicted the stress-strain response and texture evolution of low stacking fault energy (SFE) austenitic steels in both single and polycrystalline form.

It has been observed by a number of researchers that the plastic anisotropy, due to crystallographic texture, in single-phase materials can be decreased significantly when precipitates are introduced into the matrix.[18–22] A polycrystal model that is based on the Taylor assumption alone cannot predict the stress-strain curves of materials containing nonshearable precipitates, because they consider only the anisotropy in flow behavior due to crystallographic texture.[19] Specialized hardening formulations need to be developed that can account for the added precipitate-induced anisotropy and used in conjunction with polycrystal models that account for the texture anisotropy.

D. CANADINC, Graduate Research Assistant, and H. SEHITOGLU, Professor, are with the Department of Mechanical and Industrial Engineering, University of Illinois, Urbana, IL 61801. Contact e-mail: huseyin@uiuc.edu I. KARAMAN, Assistant Professor, is with the Department of Mechanical Engineering, Texas A&M University, College Station, TX 77843. Y.I. CHUMLYAKOV, Professor, is with the Siberian Physical-Technical Institute, Tomsk, 634050, Russia. H.J. MAIER, Professor, is with the University of Paderborn, Lehrstuhl für Werkstoffkunde, D-33095 Paderborn, Germany.

Manuscript submitted August 13, 2002.

Two types of models have been forwarded to account for the precipitate-induced anisotropy. In the "plastic inclusion" models, the precipitates are assumed to deform plastically.[19] On the other hand, the "elastic inclusion" models[23,24,25] treat the precipitates as impenetrable, nondeforming obstacles. It has been concluded that[20] the elastic inclusion models are more appropriate representations of precipitation-hardening systems with strong semicoherent and incoherent precipitates. In the present material, the precipitates are coarse, strong and incoherent, and do not exhibit significant deformation, as transmission electron microscopy (TEM) investigations demonstrated. Therefore, the present modeling effort will treat precipitates as impenetrable elastic obstacles. These obstacles are incorporated into the hardening formulation of a visco-plastic self-consistent (VPSC) framework producing a geometric contribution to the internal state variable evolution, which is dislocation density in the present case.

In summary, we report the role of different nitrogen levels on the deformation mechanisms, CRSS levels, and strain-hardening behavior as a function of selected crystallographic orientation. The deformation mechanisms involve slip and twinning depending on the crystal orientation and strain levels. Finally, we focus on the prediction of the stress-strain response of HS single crystals with and without nitrogen. For this purpose, a VPSC crystal plasticity model is modified by incorporating precipitate spacing and twinning length scales into a crystal plasticity formulation.

II. EXPERIMENTAL TECHNIQUES

The material used in this study is HS with a chemical composition of 12.3 wt pct Mn, 1 wt pct C, and balance Fe. The HS has an fcc crystal structure. The Bridgman technique was employed to grow single crystals on <111> seeds in magnesia crucibles in a He atmosphere. Homogenization of the single crystals was carried out at 1323 K for 20 hours. Electrodischarge machining (EDM) was used to cut compression specimens with nominal dimensions of $8 \times 4 \times 4$ mm. Nitrogen was added to the samples in two different amounts for every orientation, at 0.05 and 1.06 wt pct, respectively. In order to remove damaged surface layers, mechanical grounding, chemical etching, and electropolishing were applied to all specimens prior to the nitriding treatment. Thereafter, a solution heat treatment was conducted at 1423 K for 1 hour, followed by water quenching. To obtain HS with 0.05 wt pct N samples, nitriding was performed thermogasobarically, *i.e.*, by annealing the samples 6 to 8 hours at 1550 K under 1 atm pressure of gaseous nitrogen. Samples containing 1.06 wt pct N, on the other hand, were processed using the hot isostatic pressing technique (1273 K for 40 hours under 1200 atm).

A servohydraulic Instron (Canton, MA) 1331 test set-up equipped with an Instron 8500 controller was employed to perform the tests at room temperature with a strain rate of $4 \times 10^{-4}\ s^{-1}$. To check repeatability and consistency between results, tests were repeated on two to eight companion specimens. Transmission electron microscopy was employed to observe the microstructure at several stages of the deformation, and thereby relating the macroscopic changes to the microstructure. Prior to TEM analysis, tested samples were prepared by mechanical grinding and twin jet electropolishing. Thin foils were examined in a PHILIPS* CM 200 electron microscope operated at 200 kV. To determine the thickness and the volume fraction of twins, twins were viewed edge-on in the micrographs.

*PHILIPS is a trademark of Philips Electronic Instruments Corp., Mahwah, NJ.

III. EXPERIMENTAL RESULTS

A. *Room-Temperature Stress-Strain Response under Compressive Loading*

The room-temperature stress-strain responses of HS without nitrogen (HSw/oN), HS with low (0.05 wt pct) nitrogen concentration (LNHS), and HS with high (1.06 wt. pct) nitrogen concentration (HNHS) are reported in this section. We considered six different crystallographic orientations ([$\bar{1}$11], [001], [$\bar{1}$23], [01$\bar{1}$], [144], and [1510]) under compressive loading. The [1510] orientation represents the [1, 5, 10] orientation in the cubic structure; it should not be confused with the nomenclature used for the hcp structure. These orientations were selected to represent the different regions of the standard stereographic triangle as well as to bias the governing deformation mechanisms. For example, we would expect to observe twinning in the [001] orientations of low stacking fault energy materials under compression, while it is theoretically unexpected in the [111] . This can be partly deduced by comparing the Schmid factors of the selected orientations for twinning and slip. The experiments revealed that the stress-strain behavior depends strongly on the nitrogen concentration and crystal orientation (Figure 1). The stress-strain curves for only three orientations are given in Figures 1(a) through (c). The introduction of nitrogen into HS resulted in a significant change in the mechanical properties.

The yield strength (σ_y) levels increase drastically with increasing nitrogen concentration (Table I, Figure 1). This increase (up to 177 pct) followed the same trend for all six crystallographic orientations, even though the role of nitrogen concentration is also orientation dependent. Among the six different orientations, the [$\bar{1}$11] orientation single crystals of all three HS batches (HSw/oN, LNHS, and HNHS) demonstrated the highest strength values compared to other orientations of the same batch. Also, the critical resolved shear stress (CRSS) values increase significantly with the increasing nitrogen concentration, as shown in Table I. The CRSS values for each crystal orientation are calculated using the experimentally determined yield strength values and the corresponding fcc Schmid factors for slip or twinning.

The strain-hardening behavior is drastically influenced by the addition of 1.06 wt pct nitrogen. The HNHS single crystals exhibit a rapid strain-hardening behavior in the stage I of the plastic deformation regime, unlike the HSw/oN and LNHS single crystals. A linear stage II inelastic deformation regime was observed for single crystals of HSw/oN and LNHS batches proceeded by an upward stress-strain regime. The HNHS single crystals, on the other hand, exhibit a rapid strain-hardening behavior with significantly higher hardening coefficients than that of HSw/oN and LNHS batches, which is attributed to precipitation hardening. The rapid

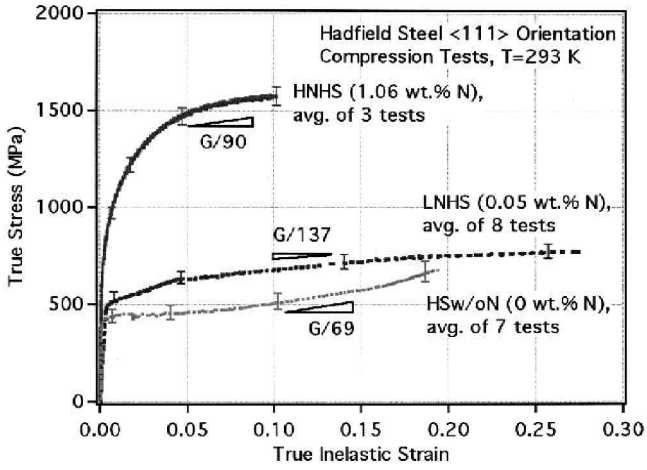

(*a*)

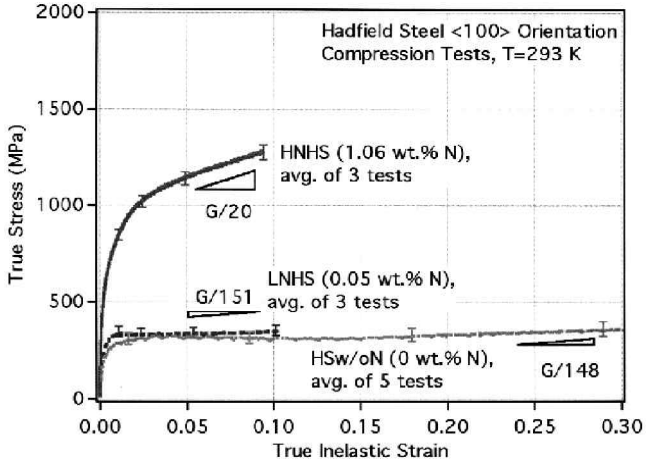

(*b*)

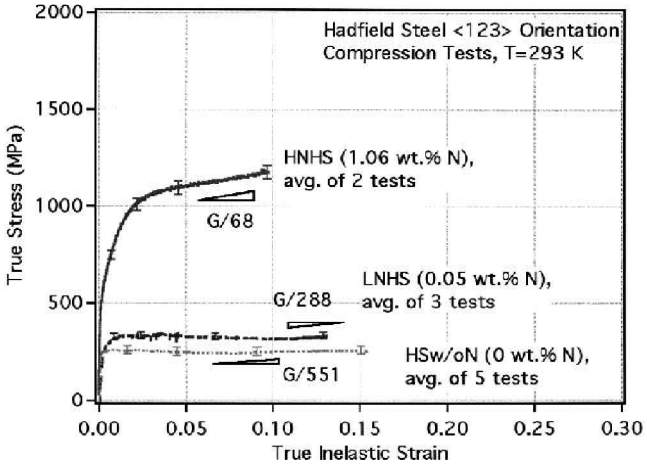

(*c*)

Fig. 1—True stress–true inelastic strain response of HS: (*a*) [$\bar{1}$11], (*b*) [001], and (*c*) [$\bar{1}$23] orientation single crystals under monotonic compressive loading at room temperature for three different nitrogen contents. Tests were stopped at finite strains.

strain-hardening regime ends with a downward hardening regime, and then the materials exhibit a hardening regime similar to stage II hardening of other batches. This saturation behavior is attributed to the start of Orowan loop relaxation around precipitates.[24] The slight change in strain-hardening coefficients in the LNHS as compared to the HSw/oN is attributed to the twin density increase with increasing the interstitial atom content. At this moment, we do not have a direct evidence for this hypothesis, but our earlier studies demonstrated that increasing the carbon content from 1.0 wt pct to 1.1 wt pct and 1.3 wt pct in HS considerably increases the twin density. We expect a similar effect with the addition of nitrogen. In summary, comparison between the stage II coefficients, θ, of deformation hardening (Table I, Figure 1) reveals the dependence of θ on the nitrogen concentration. In general, increasing nitrogen concentration led to a significant increase in θ, which is also strongly orientation dependent. The highest θ values were demonstrated by the [001], [01$\bar{1}$], and [1510] orientations with θ values of G/20, G/27, and G/37 respectively.

B. *Microstructure*

In order to gain an understanding of microstructural evolution, TEM analysis was performed on the tested samples of all orientations from each batch. The HSw/oN and LNHS single crystals of the same orientation produced similar TEM images; however, considerable changes were revealed for the HNHS batches (Figures 2 and 3). The HNHS samples exhibited large nitrides, contributing to precipitation hardening.

Precipitates were detected in HNHS samples for all six crystal orientations. Twinning was observed in all orientations (Figures 2(c) and 3(b) and (c)) due to addition of nitrogen and formation of precipitates. The twin density shows variation depending on the orientation. The [$\bar{1}$11] orientation HNHS single crystals exhibit large precipitates in the microstructure (Figure 2(a)) and display a low density of twins (Figure 2(c)). In contrast, the [001], [01$\bar{1}$], and [1510] orientated single crystals of HSw/oN, LNHS (not shown), and HNHS batches exhibit a high density of twins in the microstructure (Figure 3). As for the [$\bar{1}$23] and [144] (not shown) orientations, a relatively high density of twins was observed.

To quantitatively assess the influence of the precipitates on the mechanical behavior, the size distribution and volume fraction of precipitates may be needed. However, the size distribution was not studied explicitly in this study as several TEM images demonstrated that the shape of the precipitates is near spherical or circular plate, with small scattering in characteristic sizes. Instead, the average size is calculated to be 1 μm from these images and this is used in the subsequent analysis as a first approximation.

IV. MODELING OF STRESS-STRAIN BEHAVIOR: INCORPORATION OF PRECIPITATION AND TWINNING LENGTH SCALES INTO A VPSC MODEL

In addition to our experimental observations, in the present study, we use a VPSC formulation to predict the stress-strain response of Hadfield manganese steel single crystals with and without nitrogen alloying under compression.

Table I. Experimentally Determined (0.2 pct Offset) Yield Strengths (σ_y, MPa), CRSS (MPa) at the Onset of Yielding, and Coefficients of Deformation Hardening (θ) at the Stage II Regime for HS Single Crystals Used in This Study

Material	Parameters	<111>	<100>	<110>	<123>	<144>	<1510>
HSw/oN	σ_y	426	274	289	259	258	242
	DM	S (MSB)	T	S (MSB)	S	S (MSB)	T
	SF	0.27	0.47	0.42	0.46	0.43	0.50
	CRSS	115 ± 1	129 ± 2	121 ± 2	119 ± 2	111 ± 2	121 ± 4
	θ	G/69	G/148	G/179	G/551	G/669	G/415
LNHS	σ_y	582	314	350	295	309	263
	DM	S (MSB)	T	S (MSB)	S	S (MSB)	T
	SF	0.27	0.47	0.42	0.46	0.43	0.42
	CRSS	157 ± 4	148 ± 7	147 ± 2	136 ± 9	133 ± 4	110 ± 4
	θ	G/137	G/151	G/48	G/288	G/208	G/130
HNHS	σ_y	736	654	712	633	677	321
	DM	S (MSB)	T	S (MSB)	S	S (MSB)	T
	SF	0.27	0.47	0.42	0.46	0.43	0.42
	CRSS	199 ± 7	307 ± 8	299 ± 2	291 ± 9	291 ± 7	135 ± 2
	θ	G/90	G/20	G/27	G/68	G/47	G/37

DM: Initial macrodeformation mechanism, SF: Schmid factor, S: slip, T: twin, MSB: macroshear bands, and G: shear modulus.

Our unique strain-hardening approach incorporating length scales associated with spacing between twin lamellae and grain boundary spacing was established earlier.[16] Here, we incorporate the role of precipitation hardening and twin-slip-precipitate interaction on the strain-hardening behavior. The present modeling effort treats precipitates as impenetrable elastic obstacles that control the mean free path of dislocations, which is a reasonable approximation for the deformation conditions considered in this study. These obstacles are incorporated into the hardening formulation of VPSC, producing a geometric contribution to the internal state variable evolution, *i.e.*, dislocation density. The results will demonstrate that the model is applicable to predicting the deformation response of low SFE materials with and without precipitates undergoing twinning and slip.

The modeling is outlined as follows: in Section A, the constitutive equations for single crystals and the essentials of the VPSC formulation will be briefly described. Section B will include a detailed explanation of our hardening approach incorporating both twinning and slip, and Section C will describe how we treat the incoherent precipitates in the hardening formulation as impenetrable obstacles. Simulation results and comparison with the experiments are presented in Section D.

A. *VPSC Constitutive Formulation*

The VPSC formulation together with a twinning reoriéntation scheme was first developed by Lebensohn and Tomé.[26] The VPSC treats each grain or twin lamellae as a visco-plastic inclusion embedded in a homogeneous medium representing the polycrystalline aggregate. We present the main formulation of the VPSC model subsequently (more details can be found in References 2, 16, 17, and 26). The constitutive law for the grain is based on a rate sensitive criterion, which expresses the shear rate in each deformation system as a power of the resolved shear stress in the system. The total strain rate in a crystal can be written as the sum of all potentially active systems and can be pseudolinearized as follows[26]:

$$\dot{\varepsilon}_i = \left[\dot{\gamma}_0 \sum_1 \frac{m_i^s m_j^s}{\tau_0^s} \left(\frac{m_k^s \sigma_k}{\tau_0^s} \right)^{n-1} \right] \sigma_j = M_{ij}^{c(\mathrm{sec})}(\sigma)\sigma_j \quad [1]$$

where $\dot{\gamma}_0$ is a reference rate, τ_0^s is the threshold stress corresponding to this reference rate, n is the inverse of the rate-sensitivity index, and m and σ are the vector representations of the Schmid and the remote stress tensors, respectively. The superscript s represents the slip or twinning systems and k changes from 1 to 5 corresponding to the vector representation of the five independent components of the stress and strain rate tensors.[26] The $M_{ij}^{c(\mathrm{sec})}$ is the secant viscoplastic compliance of the crystal, which gives the instantaneous relation between stress and strain rate.

At the macroscopic level, the polycrystal response is described with the same pseudolinear constitutive equation. If the $\dot{E}$ and $\dot{\Sigma}$ are the polycrystal strain rate and stress, respectively, the secant relation can be written as

$$\dot{E}_i = M_{ij}^{(\mathrm{sec})}(\Sigma)\dot{\Sigma}_j \quad [2]$$

where $M^{(\mathrm{sec})}$ is the secant compliance tensor for the polycrystal aggregate.

The deviations in strain rate and stress between the inclusion and the overall magnitude are defined as

$$\tilde{\dot{\varepsilon}}_k = \dot{\varepsilon}_k - \dot{E}_k \quad [3]$$

$$\tilde{\dot{\sigma}}_j = \dot{\sigma}_j - \dot{\Sigma}_j \quad [4]$$

The solution of the visco-plastic inclusion problem leads to the interaction equation

$$\tilde{\dot{\varepsilon}} = -\tilde{M} : \tilde{\dot{\sigma}} \quad [5]$$

where the colon indicates tensor contraction and the interaction tensor $\tilde{M}$ is defined as

$$\tilde{M} = (\mathrm{I} - S)^{-1} : S : M^{(\mathrm{sec})} \quad [6]$$

where S is the visco-plastic Eshelby tensor.

In this formulation, the viscoplastic moduli of the grain and the homogeneous medium are assumed to be known in advance, which is not the case. Therefore, a self-consistent expression must be found from which the macroscopic modulus $M^{(\mathrm{sec})}$ can be calculated by substituting Eqs. [1]

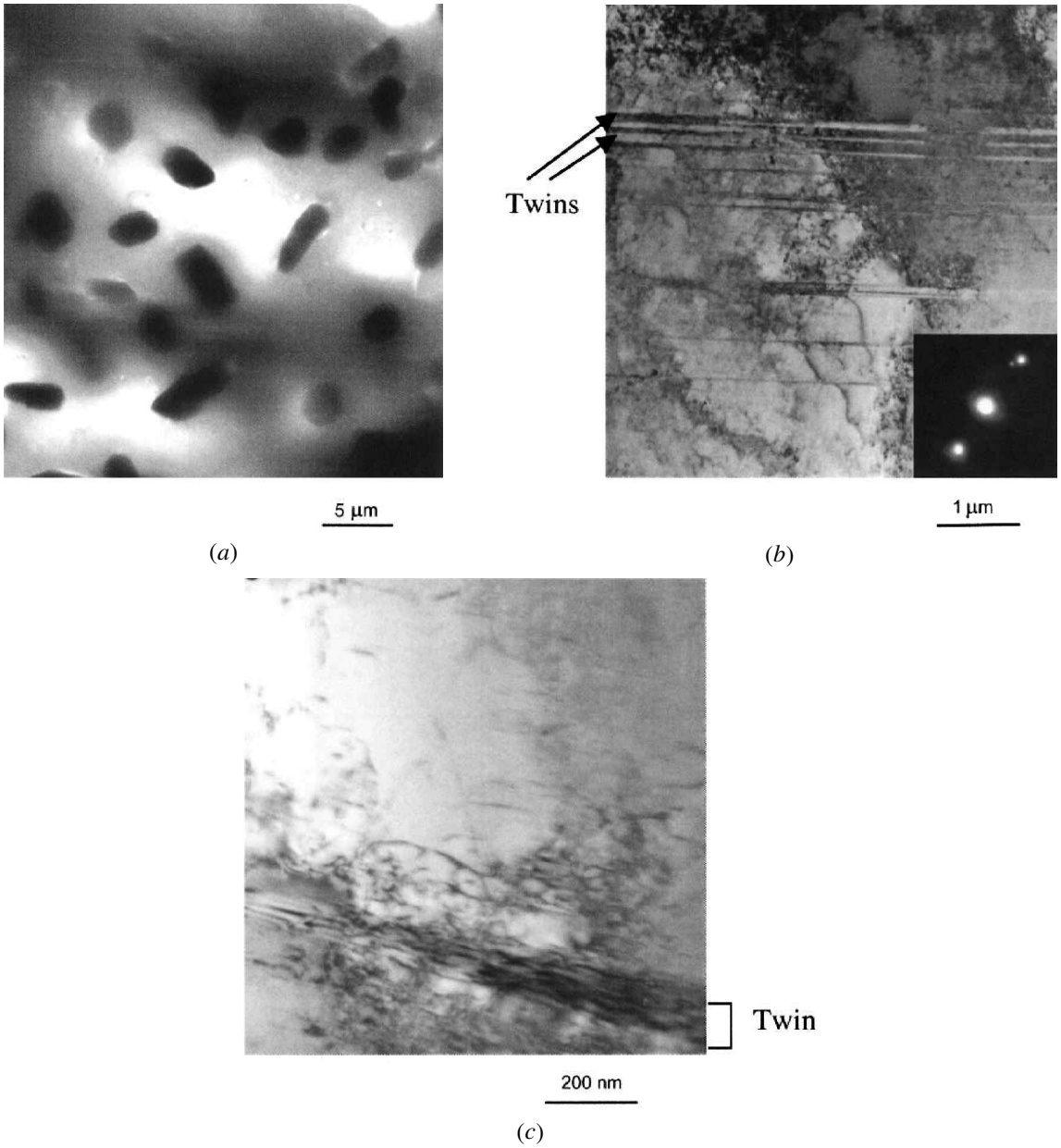

Fig. 2—(*a*) HNHS [$\bar{1}11$] orientation compressed to 5 pct strain. Very low overview showing large nitrides. (*b*) HSw/oN [$\bar{1}11$] orientation compressed to 20 pct strain. TEM image showing that twins are present. (*c*) HNHS [$\bar{1}11$] orientation compressed to 5 pct strain. TEM image showing dislocations and a twin. Note that in Figs. 2(c), and 3(b) and (c), the precipitates cannot be seen because the images were taken from interparticle spacings.

and [2] into Eq. [5]. An iterative procedure is used[16] to solve Eqs. [1], [5], and [6].

B. *Strain-Hardening Formulation*

In the present material, twinning and twin-slip interaction play a major role in the upward stress-strain response;[11] thus, the length scales associated with twinning and slip need to be taken into account in hardening. In our treatment of twinning, we consider the twin boundaries as barriers to dislocation motion.[2,16,17] Subdivision of grains during deformation by twins decreases the mean free path of dislocations proportional to the twin volume fraction. In this formulation, we consider an evolution equation for the dislocation density, ρ,[27,28] in the form

$$\dot{\rho} = \sum_k \left\{ \frac{K_0}{d\mathbf{b}} + k_1 \sqrt{\rho} - k_2 \rho \right\} |\dot{\gamma}_k| \qquad [7]$$

where d is the distance between twins, $\mathbf{b}$ is the Burgers vector, k_1 and k_2 are constants, k is the number of possible slip systems, and K_0 is a geometric constant. The first term represents an empirical geometric storage term due to twin or grain boundaries, and the second term represents the athermal (statistical) storage of moving dislocations. The dynamic recovery is represented with the third term.

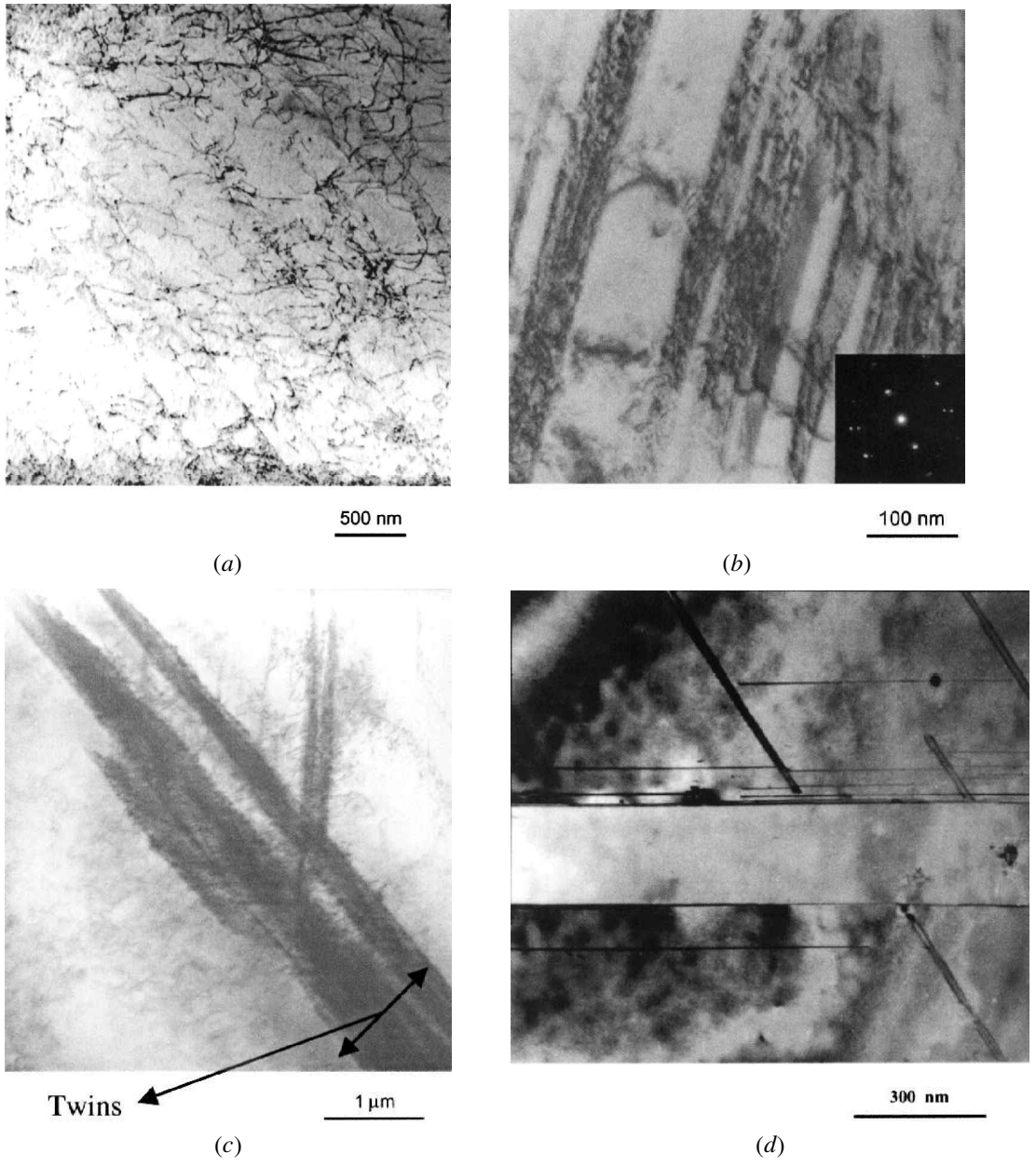

Fig. 3—(*a*) HNHS [001] orientation compressed to 4 pct strain. Two-beam image ($g = 111$) showing dislocations at intermediate magnification. Most of the dislocations tend to have a preferential orientation. (*b*) HNHS [1510] orientation compressed to 22 pct strain. TEM image showing multiple twins. (*c*) HNHS [123] orientation compressed to 4 pct strain. TEM image showing thick twins and high dislocation density in the vicinity of twins. (*d*) HSw/oN [001] orientation compressed to 3 pct strain. TEM image showing thin twins and two active twin systems.

The twins are very narrow in the present material and the spacing between twins is almost constant once twins reach a certain thickness. Thus, the mean free path is constant as well. As explained earlier, the thickness of twins depends on the chemistry of the material and the orientation of the crystals most probably because of relative slip activity in a particular orientation. As we have shown in our earlier publications,[16,17] dislocations are stored at twin boundaries and this hinders further growth of twins. The first term can also mimic the role of grain boundaries, dislocation substructures such as cell and carpet structures on the hardening. The exact form of the functional dependence on the characteristic length scale (d) is based on the type of barrier and the material. For example, in low SFE materials, it is experimentally shown that[29] the flow stress is approximately inversely proportional to the homogeneous deformation zone size. In this formulation, the barriers such as twin or cell structures that determine the mean free path of dislocations are assumed to be uniformly distributed, and any nonuniform spatial distribution as a function of strain, such as the one observed during Lüder's band formation, is not implemented.

The flow stress at a finite temperature and strain rate is defined[30] along with the Bailey–Hirsch relationship as

$$\hat{\tau}^m - \hat{\tau}_0 = \alpha\mu\mathbf{b}\sqrt{\rho} \qquad [8]$$

where $\hat{\tau}_0$ is the initial yield strength, which considers initial dislocation density, temperature, and strain rate; and α is a constant.

Upon combining Eqs. [7] and [8] and with the distance d between neighboring twins evaluated from Fullman's volumetric analysis,[31] we obtain

$$\frac{1}{d} = \frac{1}{2t}\frac{f^{tw}}{1 - f^{tw}} \qquad [9]$$

where t is the thickness of twins, and f^{tw} is the volume fraction of twins. Differentiating Eq. [8] with respect to time and combining with Eqs. [7] and [9], we obtain the following expression for single-crystal hardening:

$$\dot{\hat{\tau}}^m = \left[\frac{K_0\alpha^2\mu^2\mathbf{b}}{4(\hat{\tau}^m - \hat{\tau}_0)}\frac{1}{t}\frac{f^{tw}}{1 - f^{tw}} + \left\{\frac{\alpha\mu\mathbf{b}}{2}k_1 - k_2\frac{\hat{\tau} - \hat{\tau}_o}{2}\right\}\right]\sum_k |\dot{\gamma}^k| + \dot{\hat{\tau}}_i \qquad [10]$$

The last term is the well-known Voce form hardening, which can be written as[32]

$$\dot{\hat{\tau}}^m = \left[\frac{K_0\alpha^2\mu^2\mathbf{b}}{4(\hat{\tau}^m - \hat{\tau}_0)}\frac{1}{t}\frac{f^{tw}}{1 - f^{tw}} + \theta_0\left\{\frac{\hat{\tau}_s - \hat{\tau}}{\hat{\tau}_s - \hat{\tau}_0}\right\} + \frac{\partial\hat{\tau}_i}{\partial\gamma}\right]\sum_k |\dot{\gamma}^k| \qquad [11]$$

where θ_0 is the constant strain-hardening rate, $\hat{\tau}_s$ is the saturation stress in the absence of geometric effects, and $\hat{\tau}_i$ is the strain rate and temperature-dependent contribution of solid solution hardening.

Equation [11] can be generalized to account for other geometric storage contributions such as ones from grain, cell, or interphase boundaries as follows:

$$\dot{\hat{\tau}}^m = \left[\frac{\alpha^2\mu^2\mathbf{b}}{2(\hat{\tau}^m - \hat{\tau}_0)}\sum_s\frac{K_s}{d_s} + \theta_0\left\{\frac{\hat{\tau}_s - \hat{\tau}}{\hat{\tau}_s - \hat{\tau}_0}\right\} + \frac{\partial\hat{\tau}_i}{\partial\gamma}\right]\sum_k |\dot{\gamma}^k| \qquad [12]$$

where s corresponds to different storage mechanisms, while K_s represents the strength of the barrier or the amount of storage. Because the nature of the interaction between the last and first term has not been completely understood to date, a simple superposition is used.[30] It should be noted that, in a more general treatment, $\hat{\tau}_i$ and Eq. [12] should be modified to account for the kinetics of flow. The preceding formulation has been successfully used for predicting the stress-strain response and texture evolution of polycrystal HS[16] considering twin and grain boundaries. Its extension to austenitic stainless steel single crystals with twin and dislocation cell boundaries[2] controlling the hardening has also been implemented.

The tracking of the reorientation of a grain by twinning while storing the previous deformation history of the grain is performed by the (PTR) predominant twin reorientation scheme.[33] In this scheme, the accumulated twin volume fraction in the individual twinning systems of each grain is compared with a threshold value f_T at every deformation step, and the grain is reoriented if the twin volume fraction is above the threshold. The characteristic of this scheme is that it favors the reorientation of crystals using the most active twinning systems. This is justifiable from the experimental findings, since at most, two twin systems prevail in single crystals of HSs with and without nitrogen at small and moderate strains (Figure 3). The rest of the twinning activity is considered as pseudo-slip to satisfy compatibility conditions. This approach is shown to work well in predicting the experimental evolution of twin volume fractions with strain in the present single crystals.[16]

What follows is the incorporation of semicoherent and incoherent precipitates into this hardening formulation as barriers to dislocation motion and as sources for back-stress accumulation.

C. *Incorporation of Precipitation Hardening into the Hardening Formulation*

In the present approach, we consider precipitates modifying the critical shear stress on the slip and twinning systems. This is achieved by modifying the hardening formula (Eq. [12]) accounting for the dislocation-precipitate interaction and by considering the precipitates as one of the controlling factors of the mean free path of dislocations. As plastic strain progresses, Orowan loops are stored around the precipitates, which gives rise to long-range internal stress in the matrix. The back stress evolves rapidly at the beginning of deformation but tends to saturate with increasing strain due to plastic relaxation mechanisms around the particles during deformation, such as cross-slip, formation of prismatic dislocation loops, and dislocation annihilation.

We treat semicoherent and incoherent precipitates as elastic inclusions and follow a formulation initially similar to Bate *et al.*,[20] Brown *et al.*,[23,24,25] and Barlat and Liu.[21] Exact formulation differs in details, because we also factor back-stress accumulation with plastic relaxation and geometric storage of dislocations as a contribution to the forest hardening.

Assuming that the precipitates are elastic inclusions in the matrix, applying a uniform strain to the body that is associated with a stress, $\hat{\tau}^m$ gives the resulting average stress as

$$\hat{\tau} = (1 - f)\hat{\tau}^m + f\hat{\tau}^p \qquad [13]$$

where $\hat{\tau}^p$ is the stress of the precipitate and f is the volume fraction of precipitates.

Considering the Eshelby inclusion problem, $\hat{\tau}^p$ can be written as

$$\hat{\tau}^p = C(I - S)\gamma_p \qquad [14]$$

where I and S are the fourth-order identity and Eshelby tensors, respectively; C is the elastic modulus tensor; and γ_p is the plastic strain discontinuity at the matrix/particle interface. Technically, the value of the strain discontinuity should be less than the applied strain due to plastic relaxation around the particle after a certain amount of strain. Equation 14 can be written for spherical inclusions as[34]

$$\hat{\tau}^p = 2\mu\chi D\gamma_p^* \qquad [15]$$

where χ is the Eshelby accommodation factor, μ is the shear modulus, D is the modulus correction term, and * represents

the unrelaxed portion of the plastic strain. The value of D is orientation dependent because of the orientation dependency of the single-crystal moduli.

The anisotropy due to the precipitates is incorporated into the model by the magnitude of the accommodation factor, which is dependent upon the shape and orientation of the precipitates. The term $f\hat{\tau}^p$ opposes the applied stress during the deformation, resulting in a back stress. The back stress evolves with increasing strain and tends to saturate due to plastic relaxation. Brown and Stobbs[25] demonstrated that the plastic relaxation strain is a function of applied strain level, precipitate size, shape, and volume fraction and can be approximated for spherical precipitates as

$$\gamma_p^* = \left(\frac{8\pi \mathbf{b}}{\alpha^2 \gamma_p\, r_0}\right)^{1/8} \alpha \left(\frac{8\gamma_p \mathbf{b}}{\pi r_0}\right)^{1/2} \qquad [16]$$

where r_0 is the radius of precipitates. The first term in Eq. [13] is the stress in the matrix, which depends upon the internal state variable, the dislocation density, and can be found by using Eq. [8]. Replacing Eq. [12] and the time derivative of Eq. [16] into the time derivative of Eq. [13] results in the constitutive relation for stress evolution with plastic relaxation around particles as

$$\dot{\hat{\tau}} = \left[\left(1 - \frac{2\pi}{3}\frac{r^2}{d_3^2}\right)\left(\frac{\alpha^2\mu^2\mathbf{b}}{2\,(\hat{\tau} - \hat{\tau}_0)}\sum_{s=1}^{3}\frac{K_s}{d_s} + \theta_0\left\{\frac{\hat{\tau}_s - \hat{\tau}}{\hat{\tau}_s - \hat{\tau}_0}\right\} + \frac{\partial \hat{\tau}_i}{\partial \gamma}\right) + \pi\chi\frac{r^2}{d_3^2}\mu D A \frac{1}{\gamma^{5/8}}\right]\sum_k |\dot{\gamma}^k| \qquad [17]$$

In Eq. [17], d_1, d_2, and d_3 represent the distance between twin lamellae, grain size, and the distance between precipitates, respectively. The volume fraction of precipitates depends on the radius of precipitates and the distance between precipitates, $f^p = (2\pi/3)(r/d_3)^2$.[35] The d_1 can be expressed in terms of volume fraction of twins and the twin thickness, because the twin thickness remains constant once it reaches a critical value.[17,18] Because we attempt to predict the single-crystal response, $d_2 = 0$, and Eq. [17] becomes

$$\dot{\hat{\tau}} = \left[\left(1 - \frac{2\pi}{3}\frac{r^2}{d_3^2}\right)\left(\frac{K_1\alpha^2\mu^2\mathbf{b}}{4(\hat{\tau} - \hat{\tau}_0)}\frac{1}{t}\frac{f^{tw}}{1 - f^{tw}} + \frac{K_3\alpha^2\mu^2\mathbf{b}}{4(\hat{\tau} - \hat{\tau}_0)}\frac{1}{d_3} + \theta_0\left\{\frac{\hat{\tau}_s - \hat{\tau}}{\hat{\tau}_s - \tau_0}\right\} + \frac{\partial \hat{\tau}_i}{\partial \gamma}\right) + \pi\chi\frac{r_0^2}{d_3^2}\mu D A \frac{1}{\gamma^{5/8}}\right]\sum_k |\dot{\gamma}^k| \qquad [18]$$

The term K_3 can be considered as the strength of the precipitate/matrix interface. A is a derived parameter, which is a function of the radius of precipitates and the Eshelby accommodation factor. The second term can be considered as the factor restricting the mean free path of dislocations due to precipitates, and the last term is due to a localized elastic stress field of plastic zone around the precipitates, which acts as back stress.

Before plastic relaxation starts, the total applied strain can be considered as unrelaxed and Eq. [18] can be written as

$$\dot{\hat{\tau}} = \left[\left(1 - \frac{2\pi}{3}\frac{r^2}{d_3^2}\right)\left(\frac{K_1\alpha^2\mu^2\mathbf{b}}{4(\hat{\tau} - \hat{\tau}_0)}\frac{1}{t}\frac{f^{tw}}{1 - f^{tw}} + \frac{K_3\alpha^2\mu^2\mathbf{b}}{2(\hat{\tau} - \hat{\tau}_0)}\frac{1}{d_3} + \theta_0\left\{\frac{\hat{\tau}_s - \hat{\tau}}{\hat{\tau}_s - \tau_0}\right\} + \frac{\partial \hat{\tau}_i}{\partial \gamma}\right) + 2f\chi\mu D\right]\sum_k |\dot{\gamma}^k| \qquad [19]$$

When plastic relaxation actually starts can be determined either experimentally or by assuming that the mechanism of stress relief is by the conversion of shear loops to prismatic loops at the particles and calculating the strain level required for this conversion using Ashby's geometrically necessary dislocation approach.[36] Experimentally, it can be argued that the relaxation initiates where the macrostrain regime starts before which the unrelaxed strain around particles originates very high strain hardening in the microstrain regime (Figure 4(a)). Theoretically, the critical strain level is equal to $\gamma_p^{crit} = 2\mathbf{b}/27\, fr_0$ following Brown and Stobbs.[25] For the present case, this value is approximately 0.02 pct. As will be shown in Section D (Figure 4(a)), the experimental values are slightly larger than the calculations, which can be attributed to the added difficulty of forming prismatic loops due to interstitial solid solution hardening and short-range order.

D. *Simulations of Experimental Results*

To compare the relative roles of twinning, slip, and precipitates in HS single crystals under compression with and without nitrogen alloying, two orientations have been chosen ([001] and [$\bar{1}$11]). To predict single-crystal stress-strain response, a total number of 1000 grains was used and all grains initially had the same crystallographic orientation. This proves the scheme to be statistically meaningful. As a result of this, boundary conditions were satisfied without imposing constraints as in the case of Taylor–Bishop–Hill and relaxed constraints formulations. Stress-strain simulations were carried out using the preferred twinning reorientation and strain-hardening schemes described in Section B. Twinning is the primary deformation in the [001] orientation of the pure HS under compression. While slip governs the deformation in the [$\bar{1}$11] orientation, thin twins are also present. The effect of twinning on the strain-hardening behavior can be seen in Figures 4(a) and (b) as slip-twin interaction leads to an upward curvature. In the nitrogen-alloyed [001] and [$\bar{1}$11] crystals, twinning is also a significant deformation mechanism. However, precipitation hardening originates a very high hardening at small strains while the hardening saturates with increasing strain as the plastic relaxation progresses at higher strains, leading to a curve shape similar to stage II hardening of single crystals of pure materials. Overall, the hardening rate, even at higher strain levels, is still larger than in the crystals without nitrogen, indicating the combined effect of twinning and precipitation hardening.

With these observations, the initial CRSS for both slip and twinning are obtained from the experimental results.

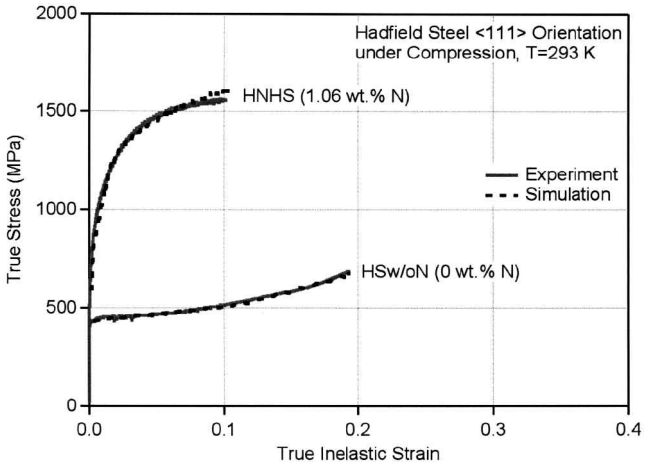

(*a*)

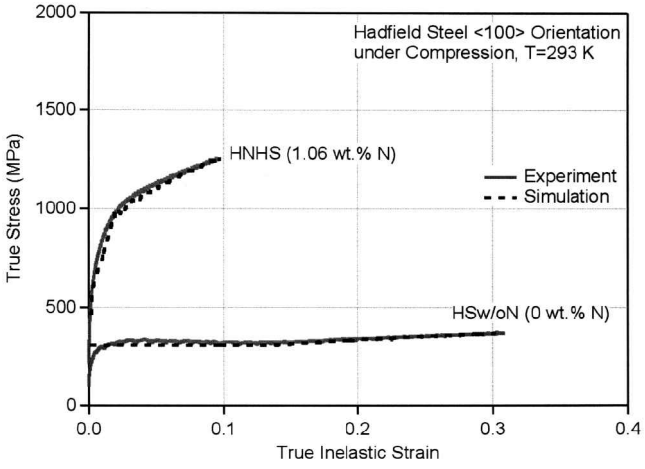

(*b*)

Fig. 4—The stress strain response of (*a*) the [$\bar{1}$11] orientation, and (*b*) the [001] orientation single crystals of HS with and without nitrogen alloying deformed under compression at room temperature. The nitrogen-alloyed crystals consist of incoherent nitrides. Both experimental results and simulations are demonstrated.

The CRSS for twinning was taken to be comparable to the one for slip since twinning is observed at very low strains (<3 pct). The rate sensitivity n is chosen to be 20. Because twinning starts at strains as low as 1 pct, the twinning activation scheme is implemented early to be consistent with the experimental findings. The initial value of the mechanical threshold was set to $\tau_0 = 140$ MPa for slip and $\tau_0 = 145$ MPa for twinning considering the requirement of multiple slip for twinning. Since twinning (intrinsic) is very difficult to nucleate in the [$\bar{1}$11] orientation because of the inherent fcc crystal structure and the low Schmid factor,[17] extrinsic twinning is allowed to form to be consistent with the experimental observations in this orientation. Twins are very narrow and remain at constant width of about 70 nm in the [$\bar{1}$11] orientation (Figures 2(b) and (c)) and 150 nm in the [001] orientation (Figure 3(d)). Therefore, the thickness t in the hardening term in Eq. [10] originating from the geometric dislocation storage is set to 70 and 150 nm, respectively. The value of α is 1/3,[37] and K_0 is 0.08 found by fitting the simulation curve to the compressive response of the [$\bar{1}$11] orientation. The value of $\partial\hat{\tau}_i/\partial\gamma$ in Eq. [12] is derived from the experimental stress-strain response of the [$\bar{1}$11] orientation. Because the initial hardening rate is small due to a Lüders-type propagation, it is taken as $\mu/4000$ for both slip and twinning following the stage I hardening contribution of interstitial solid solutions shown by Fleischer.[41]

For the nitrogen-alloyed crystals, $\tau_0 = 185$ MPa for the [$\bar{1}$11] orientation and $\tau_0 = 230$ MPa for the [001] orientation is used, which corresponds to the experimental microscopic yield. Although experimental macroscopic mechanical threshold stresses are comparable ($\tau_0^{\text{macro}} \cong 400$ MPa) for both orientations, microscopic values are different despite the fact that one would expect them to be similar. The exact reason for this discrepancy is not clear at the moment; however, it is believed to result from the effect of precipitate stress fields on the slip systems. Since semi coherent precipitates reduce the plastic anisotropy of crystallographic texture,[21] the orientation dependence of stress-strain response should decrease. It is indeed what is observed in the present experimental results.

In the case of nitrogen-alloyed crystals, the precipitation-hardening parameters are chosen in such a way that the original parameters found in nitrogen-free crystals were maintained constant, and the precipitation-hardening parameters are fit to predict the stress-strain response. The accommodation factor χ is taken to be 0.4 for multiple slip orientations (from Table IV of Reference 38) considering the component of the Burgers vector of a slip system perpendicular to precipitates. The K_1 is kept constant as 0.08 and K_3 is taken as 0.1. The d_3 and r_0 are determined from TEM images as 4 and 1 μm (Figure 2(a)), respectively, resulting in the volume fraction of precipitates as approximately 13 pct. The precipitates are assumed to be spherical and randomly oriented. From this volume fraction, the theoretical critical strain for plastic relaxation to commence is calculated to be 0.02 pct. However, this value was quite low to predict the experimental results. Therefore, the transition strain from microstrain regime to macrostrain regime is taken as the critical strain for plastic relaxation, which is approximately 1.5 pct. To find out a more precise critical strain value, *in-situ* TEM investigations, or a detailed dislocation analysis at small strain increments should be carried out. The modulus correction term, D, is a function of the shear moduli ratio of precipitates and the matrix, and was taken as 1.2 for the present case.[24]

The corresponding simulations for the aforementioned cases are presented in Figures 4(a) and (b) for pure and nitrogen-alloyed HSs, respectively. There is a good agreement between the experimental results and prediction for these four cases. In the [$\bar{1}$11] orientation of the pure HS, one twinning system is primarily active in predictions with a small secondary twinning formation at the later stages of deformation. The multiple slip activity and slip-twin interaction led to an upward stress-strain response, which is also the case for experimental observations. This has been shown in our previous publications in more detail.[11] One important observation was that the addition of nitrogen and the formation of precipitates did not suppress twinning, contrary to our expectations. In the nitrogen-alloyed case, the precipitates govern the deformation and strain hardening, as evidenced by the downward stress-strain response in both orientations. If slip-twin or twin-twin interaction were the primary mechanism of hardening, an upward stress-strain

response would be expected, as in the case of nitrogen-free crystals. However, the precipitation-hardened nitrogen-alloyed crystals still exhibit very high hardening rates comparable to or higher than nitrogen-free crystals (HSw/oN). This indicates the efficiency of precipitates in determining the mean free path of dislocations and the strength of the matrix/precipitate interface.

The hardening coefficients of nitrogen-free and high nitrogen-alloyed crystals are quite different in the stage II hardening regime. Intrinsic twinning in the $[\bar{1}11]$ orientation under compression is theoretically impossible, and growth of twin nuclei requires a higher stress level than the one in the [001] orientation of the HSw/oN batch. Moreover, because the twin volume fraction is expected to be higher in the [001] orientation, twin-precipitate interaction can be argued to originate a higher hardening rate in the [001] orientation of nitrogen-alloyed crystals.

The present combined treatment of precipitates, twinning, and slip is unique in the sense that the formulation developed can be used to predict stress-strain response with nonproportional strain paths, such as for the prediction of the Bauschinger effect, as outlined in an earlier article.[17] Please note that although twinning and slip are incorporated into the strain-hardening formulation as two different mechanisms in the present work, the approach does not imply that twinning and slip are two separated processes. Indeed, they are inter-related because slip is required for the nucleation of twins. However, our approach does not deal with the nucleation.

V. FINAL OBSERVATIONS

The experiments revealed that the stress-strain behavior and the mechanical properties of single crystals of HSw/oN, LNHS, and HNHS batches depend strongly on the crystal orientation. Among the six selected crystallographic orientations, the highest σ_y values and strength levels are demonstrated by the $[\bar{1}11]$ orientation, which is easily distinguishable from the others (Figures 1(a) through (c)).

The addition of nitrogen provided a significant increase in CRSS and stage II strain-hardening coefficient, as noted in Table I. This indicates that nitrogen is a more effective strengthening atom than carbon. This can be attributed to the difference between size and modulus misfit of nitrogen and carbon atoms[39] with the matrix. Moreover, although there is no direct proof, it is believed that nitrogen can decrease the SFE at low (0.05 pct) and high nitrogen (1.0 pct) contents and can lead to higher twin volume fraction as in the case of very low SFE materials.[40] Therefore, the interaction of perfect dislocations and twinning partials with a high density of twin boundaries originates high strain hardening.

Another role of alloying with nitrogen is observed to be the drastic change of the strain-hardening behavior. A comparison between the stage II coefficients of deformation hardening (θ) revealed that the $[01\bar{1}]$, [001], and [1510] orientations demonstrate the highest θ values for all three compositions of HS. Among the HNHS single crystals, where the nominal nitrogen concentration is the highest, the $[\bar{1}11]$ orientation is observed to possess the lowest θ values, although its strength is superior to those of other the orientations.

The stress-strain response of all HNHS single crystals suggests that precipitation hardening is responsible for the rapid dynamic strain-hardening behavior observed in stage I of the plastic deformation. The TEM analysis revealed that HNHS single crystals possess relatively large precipitates, supporting this concept. A careful inspection of the microstructure also showed that the main difference between the microstructures of $[0\bar{1}1]$, [001], and [1510] orientation single crystals and $[\bar{1}11]$ single crystals of HNHS is the density of twins present in the microstructure (Figures 3(b) and (c)). In the $[\bar{1}11]$ orientation, twinning is rather limited, and in the $[01\bar{1}]$, [001], and [1510] orientations, twin density is observed to be relatively high. The $[\bar{1}23]$ and [144] orientation single crystals, which demonstrate higher θ values than the $[\bar{1}11]$ orientated single crystals, also exhibit a higher twin density. However, both the twin densities and θ values are lower than those of the other three orientations. Accordingly, it may be argued that the slope of the upward curvature (θ values) in the stage II regime of plastic deformation is dependent on the twin density. The coexistence of precipitates and twins promotes rapid strain hardening, *i.e.*, a high stage II coefficient of deformation hardening, which increases with increasing twin density in the microstructure.

As for the LNHS single crystals, the stress-strain response and the strain hardening of the single crystals do not exhibit a drastic difference compared to those of HSw/oN single crystals. Both batches demonstrate a constant coefficient of deformation hardening in stage I of the plastic regime, unlike the HNHS single crystals.

The current model showed that it is feasible to treat precipitates as impenetrable elastic obstacles that control the mean free path of dislocations. The twinning length scales were incorporated to the model, which is applicable to predicting the deformation of low SFE materials with and without precipitates exhibiting twinning and slip. The excellent agreement between the experiments and simulations proved this approach to be feasible.

VI. CONCLUSIONS

In the present study, single crystals of HS with various nitrogen contents have been investigated. The effect of solid solution hardening due to alloying with nitrogen on the compressive stress-strain response and the role of precipitates has been established. The following conclusions may be drawn based on this work.

1. The addition of nitrogen resulted in a drastic increase in yield strength levels. These values are observed to increase with increasing nitrogen concentration. Strength levels, CRSS values, and the change in these mechanical properties due to nitrogen addition are strongly orientation dependent. This orientation dependence, however, follows the same trend for each composition of HS studied.
2. The HNHS single crystals exhibit a rapid strain hardening behavior in the stage I of the plastic deformation regime, unlike the HSw/oN and LNHS single crystals. An increase in the stage II coefficients of deformation hardening is observed with increasing nominal nitrogen concentration.

3. The difference between the stage II coefficients of deformation hardening of HNHS single crystals is attributed to the additional hardening contributions from the precipitates and twins.
4. A VPSC model was modified to account for precipitation and twinning length scales in HS with and without nitrogen. The model showed that it is feasible to treat incoherent precipitates in the hardening formulation as factors affecting the mean free path of dislocations. The model also accounts for plastic relaxation of precipitates with increasing strain. This approach resulted in excellent agreement with experimental results for HS with and without nitrogen.

ACKNOWLEDGMENTS

This work was supported by National Science Foundation Contract No. CMS 99-00090, Mechanics of Materials Program, Directorate of Engineering (Arlington, VA). The part of the research conducted at Texas A&M University was supported by National Science Foundation Contract No. CMS 01-34554, Solid Mechanics and Materials Engineering Program, Directorate of Engineering. Dr. Carlos Tomé, MST-8, Los Alamos National Laboratory, is thanked for kindly offering his VPSC code.

REFERENCES

1. J.W. Simmons: Ph.D. Dissertation, Oregon Graduate Institute of Science and Technology, Portland, Oregon 1993.
2. I. Karaman, H. Sehitoglu, H.J. Maier, and Y.I. Chumlyakov: *Acta Mater.*, 2001, vol. 49, p. 3919.
3. K.J., Irvine, D.T. Llewellyn, and F.B. Pickering: *J. Iron Steel Inst.*, 1961, vol. 199, p. 153.
4. M.L.G. Byrnes, M. Grujicic, and W.S. Owen: *Acta Metall.*, 1987, vol. 35, p. 1853.
5. R.P. Reed: *JOM*, 1989, vol. 41, p. 16.
6. Y.I. Chumlyakov, A.D. Korotaev: *Russ. Phys. J.*, 1992, vol. 35 (9), p. 783.
7. Y.I. Chumlyakov and I.V. Kireeva, and O.V. Ivanova: *Thr. Phys. Met. Metallogr.*, 1994, vol. 78 (3), p. 350.
8. Y.I. Chumlyakov, I.V. Kireeva, A.D. Korotaev, E.I. Litvinova, and Y.L. Zuev: *Russ. Phys. J.*, 1996, vol. 39 (3), p. 189.
9. Y.I. Chumlyakov, I.V. Kireeva, H. Sehitoglu, E.I. Litvinova, E.G. Zaharova, and N.V. Luzginova: *5th Int. Conf. on High Nitrogen Steels*, Espoo, Finland, and Stockolm, Sweden, May 24–29, 1998.
10. I. Karaman, H. Sehitoglu, Y.I. Chumlyakov, H.J. Maier, and I.V. Kireeva: *Scripta Mater.*, 2001, vol. 44, p. 337.
11. I. Karaman, H. Sehitoglu, K. Gall, Y.I. Chumlyakov, and H.J. Maier: *Acta Mater.*, 2000, vol. 48, p. 1345.
12. V.G. Gavriljuk and H. Berns: *High Nitrogen Steels*, Springer-Verlag, Berlin, 1999.
13. R.A. Lebensohn and C.N. Tomé: *Mater. Sci. Eng. A*, 1994, vol. 175, p. 71.
14. A. Staroselsky and L. Anand: *J. Mech. Phys. Solids*, 1998, vol. 46, p. 671.
15. S.R. Kalindindi: *Int. J. Plasticity*, 1998b, vol. 14, p. 1265.
16. I. Karaman, H. Sehitoglu, A.J. Beaudoin, Y.I. Chumlyakov, H.J. Maier, and C.N. Tome: *Acta Mater.*, 2000, vol. 48, p. 2031.
17. I. Karaman, H. Sehitoglu, Y.I. Chumlyakov, H.J. Maier, and I.V. Kireeva: *Metall. Mater. Trans. A*, 2001, vol. 32A, p. 695.
18. S.H. Choi and F. Barlat: *Scripta Mater.*, 1999, vol. 41, p. 981.
19. W.F. Hosford and R.H. Zeisloft: *Metall. Trans.*, 1972, vol. 3, pp. 113-21.
20. P. Bate, W.T. Roberts, and D.V. Wilson: *Acta Metall. Mater.*, 1981, vol. 29, p. 1797.
21. F. Barlat and J. Liu: *Mater. Sci. Eng. A*, 1998, vol. A257, p. 47.
22. M.H. Lyttle and J.A. Wert: *Metall. Mater. Trans. A.*, 1999, vol. 30, pp. 1283-88.
23. L.M. Brown and G.R. Woolhous: *Phil. Mag. A.*, 1970, vol. 21, p. 329.
24. L.M. Brown and W.M. Stobbs: *Phil. Mag.*, 1971a, vol. 23, p. 1185.
25. L.M. Brown and W.M. Stobbs: *Phil. Mag.*, 1971b, vol. 23, p. 1201.
26. R. Lebensohn and C.N. Tomé: *Acta Metall. Mater.*, 1993, vol. 41, p. 2611.
27. Y. Estrin and H. Mecking: *Acta Metall.*, 1984, vol. 32, p. 57.
28. A. Acharya and A.J. Beaudoin: *J. Mech. Phys. Solids*, 2000, vol. 48, p. 2213.
29. E. El-Danaf, S.R. Kalidindi, and R.D. Doherty: *Metall. Mater. Trans. A.*, 1999, vol. 30A, p. 1223.
30. U.F. Kocks, A.S. Argon, and M.F. Ashby: *Progr. Mater. Sci.*, 1975, vol. 19, p. 1.
31. L. Remy: *Acta Metall.*, 1978, vol. 26, p. 443.
32. U.F. Kocks, C.N. Tomé, and R.H. Wenk: *Texture and Anisotropy*, Cambridge University Press, Cambridge, United Kingdom, 1998.
33. C.N. Tomé, R.A. Lebensohn, and U.F. Kocks: *Acta Metall. Mater.*, 1991, vol. 39, p. 2667.
34. T. Mura: *Micromechanics of Defects in Solids*, Kluwer Academic Pub., Dordrecht, The Netherlands, 1993.
35. E. Nembach: *Particle Strengthening of Metals and Alloys*, John Wiley & Sons, Inc., New York, NY, 1997.
36. M.F. Ashby: *Phil. Mag.*, 1970, vol. 14, p. 1157.
37. F.R.N. Nabarro, Z.S. Basinski, and D.B. Holt: *Adv. Phys.*, 1964, vol. 13, p. 193.
38. L.M. Brown and D.R. Clarke: *Acta Metall.*, 1975, vol. 23, p. 821.
39. H. Ino, K. Oda, and K. Umezu: *J. Jpn. Inst. Met.*, 1989, vol. 53, p. 372.
40. N. Narita and J. Takamura: in *Dislocations in Solids*, F.R.N. Nabarro, ed., North Holland Publication Co., Amsterdam, Netherlands, 1992, vol. 9, p. 135.
41. R.L. Fleischer: *Acta Metall.*, 1963, vol. 11, p. 203.